

ChemComm

Accepted Manuscript



This is an *Accepted Manuscript*, which has been through the Royal Society of Chemistry peer review process and has been accepted for publication.

Accepted Manuscripts are published online shortly after acceptance, before technical editing, formatting and proof reading. Using this free service, authors can make their results available to the community, in citable form, before we publish the edited article. We will replace this *Accepted Manuscript* with the edited and formatted *Advance Article* as soon as it is available.

You can find more information about *Accepted Manuscripts* in the [Information for Authors](#).

Please note that technical editing may introduce minor changes to the text and/or graphics, which may alter content. The journal's standard [Terms & Conditions](#) and the [Ethical guidelines](#) still apply. In no event shall the Royal Society of Chemistry be held responsible for any errors or omissions in this *Accepted Manuscript* or any consequences arising from the use of any information it contains.



ChemComm

COMMUNICATION

Characterization of a Heterobimetallic Nonheme Fe(III)-O-Cr(III) Species Formed by O₂ Activation

Received 00th January 20xx,
Accepted 00th January 20xx

Ang Zhou,^a Scott T. Kleespies,^a Katherine M. Van Heuvelen^{a,†} and Lawrence Que, Jr.^a

DOI: 10.1039/x0xx00000x

www.rsc.org/

We report the generation and spectroscopic characterization of a heterobimetallic [(TMC)Fe^{III}-O-Cr^{III}(OTf)₄] species (1**) by O₂ bubbling into a mixture of Fe(TMC)(OTf)₂ and Cr(OTf)₂ in NCCH₃. Complex **1** also formed quantitatively by adding Cr(OTf)₂ to [Fe^{IV}(O)(TMC)(NCCH₃)]²⁺. The proposed O₂ activation mechanism involves the trapping by a Cr-O₂ adduct by Fe(TMC)(OTf)₂.**

Oxygen activation is generally carried out by metalloenzymes with mononuclear or homodinuclear iron or copper active sites.¹⁻³ However there are two notable exceptions to this generalization, namely the heme/copper center of cytochrome oxidase essential for mammalian respiration^{1,4,5} and the nonheme Fe–O–Mn center of Class 1c ribonucleotide reductases found in pathogenic bacteria.^{6,7} There has been significant progress in obtaining synthetic models for the heme/copper center of cytochrome oxidase,⁸⁻¹⁰ but less effort has been devoted to the synthesis of nonheme (μ -oxo)heterobimetallic complexes. In 1992 Wieghardt described a series of carboxylate-bridged (TACN)Fe^{III}–O–M(Me₃TACN) (M = Cr^{III} or Mn^{III}, TACN = 1,4,7-triazacyclononane, Me₃TACN = 1,4,7-trimethyl-1,4,7-triazacyclononane) complexes obtained by hydrolysis between FeCl₃(TACN) and MCl₃(Me₃TACN) precursors.¹¹ More recently, Fukuzumi and Nam reported the crystal structure of a novel Fe^{III}–O–Sc^{III} complex, which was obtained from the reaction of [Fe^{IV}(O)(TMC)(NCCH₃)]²⁺ (TMC = 1,4,8,11-tetramethylcyclam) with Sc(OTf)₃.¹² However, no synthetic nonheme Fe–O–M complex (where M is a non-iron metal) has thus far been generated by O₂ activation. Here we report the characterization of [(TMC)Fe^{III}–O–Cr^{III}(OTf)₄] (**1**) formed by oxygenating a mixture of Fe(TMC)(OTf)₂ and Cr(OTf)₂ in CH₃CN at -40 °C or reacting [Fe^{IV}(O)(TMC)(O)](OTf)₂ with 1 eq. of Cr(OTf)₂. Bubbling O₂ into a solution of 1 mM Fe(TMC)(OTf)₂ and 1 mM Cr(OTf)₂ in CH₃CN at -40 °C rapidly elicited a UV-vis

spectrum with bands at 358, 398, 447 and 558 nm (Fig 1), suggesting the formation of a new species designated as **1**. This spectral pattern was not observed in the absence of either Fe(TMC)(OTf)₂ or Cr(OTf)₂ from the reaction mixture; Fe(TMC)(OTf)₂ simply did not react with O₂, but the reaction of Cr(OTf)₂ with O₂ gave rise to features at 358 and 445 nm (Fig 1), distinct from those of **1**. Species **1** had a half-life of 10 h at -40 °C and rapidly decayed upon warming to RT. Taken together, these observations implicate both Fe and Cr in the formation of **1**.

ESI-MS analysis of the solution of **1** at -40 °C revealed dominant peaks at m/z 461.2 (positive mode) and 514.8 (negative mode) (Fig S1), which were not observed in oxygenated solutions lacking either Fe(TMC)(OTf)₂ or Cr(OTf)₂. The ions observed have masses and isotope distribution patterns that correspond to [Fe(TMC)(OTf)]⁺ and [CrO(OTf)₃]⁻, respectively. Furthermore, the [CrO(OTf)₃]⁻ peak was upshifted by 2 units when ¹⁸O₂ was used, showing the incorporation of an oxygen atom from O₂ (Fig S2). Based on these results, we tentatively assign **1** as a heterobimetallic [(TMC)Fe^{III}–O–Cr^{III}(OTf)₄] complex, which undergoes homolysis of the Fe–O bond to give rise to the observed mass spectral features.

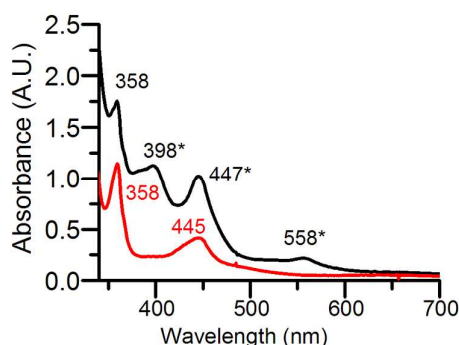


Fig 1 UV-vis spectra observed in CH₃CN at -40 °C upon O₂ exposure of 1 mM Cr(OTf)₂ (red) and a mixture of 1 mM Fe(TMC)(OTf)₂ and 1 mM Cr(OTf)₂ (black). Bands with asterisks are associated with **1**.

^a Department of Chemistry and Center for Metals in Biocatalysis, University of Minnesota, 207 Pleasant St. SE, Minneapolis, Minnesota 55455, United States

[†] Current address: Department of Chemistry, Harvey Mudd College, Claremont, CA 91711, United States.

Electronic Supplementary Information (ESI) available: Instrumental methods, synthetic procedures, and structural characterization. See DOI: 10.1039/x0xx00000x

To test this hypothesis, we investigated the reaction of $[\text{Fe}^{\text{IV}}(\text{O})(\text{TMC})(\text{NCCH}_3)]^{2+}$ with $\text{Cr}(\text{OTf})_2$ in CH_3CN at -40°C as a more direct means of synthesizing putative species **1**. As shown in Fig 2, the addition of $\text{Cr}(\text{OTf})_2$ to $[\text{Fe}^{\text{IV}}(\text{O})(\text{TMC})(\text{NCCH}_3)]^{2+}$ in CH_3CN solution caused the instantaneous disappearance of its characteristic 824-nm peak concomitant with the growth of bands at 398, 447, and 558 nm that are assigned to **1**. Titration experiments (Fig 2 inset) revealed that the transformation was complete upon addition of 1 eq. $\text{Cr}(\text{OTf})_2$, strongly suggesting a 1:1 Fe:Cr stoichiometry for **1**. This solution also gave rise to ESI-MS spectra with the same dominant peaks as the complex generated by O_2 activation. A control experiment between $\text{Cr}(\text{OTf})_2$ and PhIO did not elicit the same peaks as found in **1** (Fig S3), suggesting that $[\text{Fe}^{\text{IV}}(\text{O})(\text{TMC})(\text{NCCH}_3)]^{2+}$ acts more than just an oxygen atom donor to $\text{Cr}(\text{OTf})_2$. These results demonstrate that **1** can be generated by either O_2 activation or inner-sphere electron transfer.

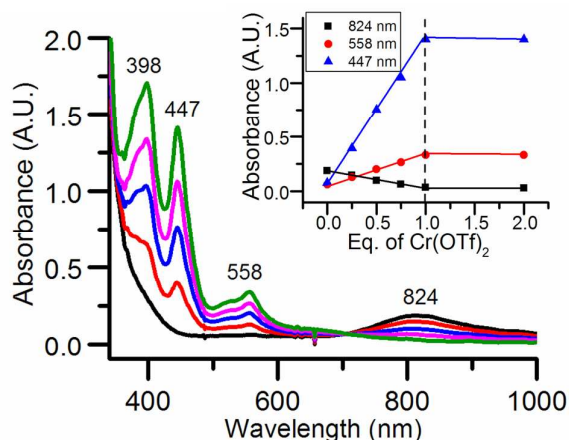


Fig 2 UV-vis spectral titration of 0.45 mM $[\text{Fe}^{\text{IV}}(\text{O})(\text{TMC})(\text{NCCH}_3)]^{2+}$ in CH_3CN at -40°C with $\text{Cr}(\text{OTf})_2$. Black, 0 eq.; red, 0.25 eq.; blue: 0.5 eq.; magenta, 0.75 eq.; green, 1 eq. Inset: titration plot. Inset: Formation of **1** vs eq. $\text{Cr}(\text{OTf})_2$ added into 0.45 mM $[\text{Fe}^{\text{IV}}(\text{O})(\text{TMC})(\text{NCCH}_3)]^{2+}$ in CH_3CN at -40°C .

In order to obtain structural insight, Fe K-edge X-ray absorption spectroscopy studies were carried out on **1**. As shown in Fig S4, the Fe K-edge of **1** was found at 7124.0 eV, which is comparable to those of known $\text{Fe}^{\text{III}}(\text{TMC})$ and related complexes.¹⁴ Species **1** also exhibits a pre-edge feature that is associated with 1s-to-3d transitions with an area of 11 units. The Fourier-transformed EXAFS region revealed two prominent features at $R + \Delta \sim 1.8 \text{ \AA}$ and 3.2 \AA (Fig 3 left). The best fit of the data (fit #8 in Table S1) consisted of 1 O/N scatterer at 1.81 \AA , 5 O/N scatterers at 2.17 \AA , 4 C scatterers at 2.91 \AA and a Cr scatterer at a distance of 3.65 \AA . The 2.17-\AA and 2.92-\AA scatterers arise from the supporting TMC ligand, while the 1.81-\AA scatterer has an Fe–O distance typically found for oxo bridges in $\text{Fe}^{\text{III}}\text{–O–M}^{\text{III}}$ complexes.¹⁵ The 3.2 \AA feature corresponds to a Cr scatterer at 3.65 \AA ; its intensity derives from multiple scattering pathways due to a linear Fe–O–Cr core. Indeed, the Fe...Cr distance is typical of the metal-metal distances found for linear $\text{Fe}^{\text{III}}\text{–O–M}^{\text{III}}$ complexes^{12,16,17} and exemplified by $[(\text{py})(\text{TPP})\text{Cr}^{\text{III}}\text{–}$

$\text{O–Fe}^{\text{III}}(\text{TMP})]$ ($r(\text{Fe}^{\text{III}}\text{...Cr}) = 3.60 \text{ \AA}$; py = pyridine; TPP = tetraphenylporphin dianion; TMP = tetramesitylporphin dianion).¹⁸ We thus propose that **1** has the structure shown in Fig 3 right.

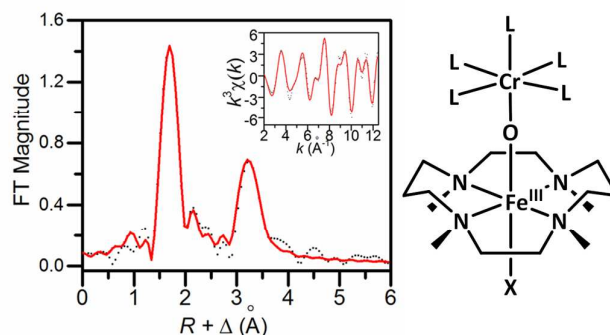


Fig 3 Left: Fourier-transformed Fe K-edge EXAFS data for **1** (dotted black line) and corresponding best fit (solid red line, fit #8 in Table S1). Inset shows unfiltered k -space data and its fit. Right: Proposed structure for **1** ($L = \text{CH}_3\text{CN}$ or OTf ; $X = \text{CH}_3\text{CN}$, NCO or NCS).

The proposed structure for **1** resembles that found in the crystal structures of the recently described $[(\text{TMC})\text{Fe}^{\text{III}}\text{–O–Sc}^{\text{III}}(\text{OTf})_4(\text{L})]$ complex (**2**, $L = \text{H}_2\text{O}$ or NCCH_3).¹² However, they differ in several respects. Although the Fe...M distances are essentially identical for **1** and **2**, the respective Fe–O and M–O distances are distinct. The Fe–O distance of 1.81 \AA for **1** is 0.07 \AA longer than that found for **2**, while the Cr–O distance of 1.84 \AA (deduced from the difference between the Fe...Cr and the Fe–O distances from the EXAFS analysis, assuming $\angle\text{Fe–O–Cr} \sim 180^\circ$) is 0.07 \AA shorter than the Sc–O distance of 1.91 \AA observed for **2** in its crystal structures. The distinct M–O distances in **1** and **2** presumably reflect the difference between the more covalent Cr–O bond and the more ionic Sc–O bond, which also affect the corresponding Fe–O bond. Another feature distinguishing **1** from **2** is the intensity of the XAS pre-edge feature. Complex **1** exhibits a pre-edge area of 11 units, typical of a six-coordinate iron(III) center,^{19,20} while **2** ($L = \text{NCCH}_3$) has a much larger pre-edge area of 32 units,²² reflecting the square pyramidal geometry of its iron(III) center. Lastly, the four methyl groups of the TMC ligand are shown in Fig 3 right as being oriented *anti* with respect to the oxo bridge, opposite to the orientation found crystallographically for the methyl groups in **2**.¹² Although we do not have direct proof, our main argument to favor the *anti* orientation over the *syn* one is the observed immediate formation of **1** upon $\text{Cr}(\text{OTf})_2$ addition to a solution of $[\text{Fe}^{\text{IV}}(\text{O})(\text{TMC})(\text{NCCH}_3)]^{2+}$. As the TMC methyl groups are oriented *anti* to the oxo moiety in the precursor,¹³ it seems unlikely that a change in their relative orientations could occur at -40°C within this very short time scale.

The likelihood of a sixth ligand for the iron(III) center in **1** is supported by the change in the spectral features of **1** upon addition of NCS^- or NCO^- . As shown in Fig 4, there are small shifts of the three bands, as well as increases in intensity. Titration experiments showed that only 1 eq. of NCS^- or NCO^- was needed to transform **1** fully into **1-NCS** or **1-NCO** (Fig S5, S6). ESI-MS analysis of **1-NCS** and **1-NCO** revealed respective positive mode peaks at m/z 370 and 354, corresponding to $[\text{Fe}(\text{TMC})(\text{NCS})]^+$ and $[\text{Fe}(\text{TMC})(\text{NCO})]^+$ fragment

ions (Fig S7, S8), suggesting the occupation of the axial position *trans* to the oxo bridge by these anions. Furthermore, **1-NCS** exhibits an Fe K-edge energy of 7124.3 eV, comparable to the 7124.0 eV value found for **1**. **1-NCS** also exhibits a pre-edge feature with an area of 9 units (Fig S9), which is close to the 11 units found for **1** but much smaller than the 32 units associated with **2**, showing that a six-coordinate iron(III) center in **1-NCS** is maintained. EXAFS analysis of **1-NCS** shows the presence of a linear Fe–O–Cr core like that in **1**, but with a 1.85 Å Fe–O bond and an Fe...Cr distance of 3.67 Å (Table S2, Fig S10). The observed lengthening of the Fe–μ-O bond can be rationalized by the axial NCS[−] binding to the iron(III) center. Based on all the information above, **1** is proposed to be a heterobimetallic μ-oxo species with a Fe–O–Cr core, and the Fe atom has a 6-coordinate environment with the axial position available for ligand substitution (Fig 3 right).

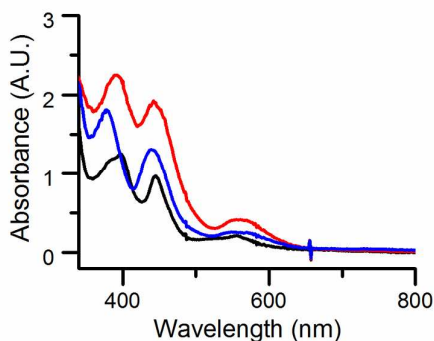


Fig 4 UV-vis spectra of 0.3 mM **1** (black), **1-NCO** (blue), **1-NCS** (red) in CH₃CN at -40 °C. λ_{max} (ϵ_{M}) for **1**: 398 (3800), 447 (3000), and 558 (700). λ_{max} (ϵ_{M}) for **1-NCO**: 380 (6000), 438 (4200), and 560 (850). λ_{max} (ϵ_{M}) for **1-NCS**: 390 (7500), 442 (6300), and 560 (1400).

Complex **1** was further studied by EPR and resonance Raman spectroscopy. It is EPR-silent, which is as expected due to antiferromagnetic coupling mediated by the oxo bridge between the Fe(III) and the Cr(III) centers, as seen for two other Fe(III)–O–Cr(III) complexes.^{11, 18} Excitation of **1** with a 568.2-nm laser elicits a resonance-enhanced vibration at 773 cm^{−1} (Fig 5), which falls within the 700–900 cm^{−1} range found for the $\nu_{\text{as}}(\text{Fe-O-Fe})$ modes of oxo-bridged diiron(III) complexes.²¹ This assignment is corroborated by the observed downshift of this vibration to 730 cm^{−1} upon ¹⁸O-substitution into the oxo bridge. Although a 35-cm^{−1} downshift for a diatomic Fe–O mode is predicted by Hooke's Law, the experimentally obtained ¹⁸O shift is 43 cm^{−1}. This larger than predicted shift has also been reported for corresponding vibrations of several oxo-bridged diiron(III) complexes.²¹ There is also a weaker feature found at 746 cm^{−1} that exhibits an upshift of 7 cm^{−1} upon ¹⁸O-substitution; this is an unusual observation that we cannot explain. The 773-cm^{−1} vibration is also weakly enhanced upon 514.5-nm excitation but not observed with 457.9 or 647.1 nm irradiation, suggesting that the 558-nm absorption band can be associated with a transition of the Fe–O–Cr moiety.

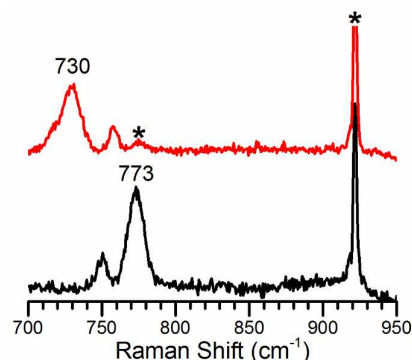
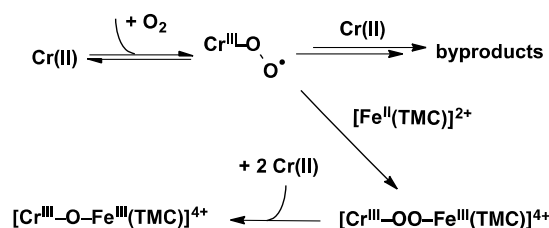


Fig 5 Resonance Raman spectra of **1** in CH₃CN (λ_{ex} = 568.2 nm, 20 mW, 77 K). Black, ¹⁶O; red, ¹⁸O. Asterisks denote solvent peaks.

With the nature of **1** reasonably well characterized, we return to an analysis of the O₂ activation reaction results. Based on the molar extinction coefficients of **1** determined from the stoichiometric conversion of [Fe^{IV}(O)(TMC)(NCCH₃)₂]²⁺ to **1** by Cr(OTf)₂, we conclude that **1** is produced in about 30% yield from the reaction of equimolar amounts of Fe(TMC)(OTf)₂ and Cr(OTf)₂ to O₂. The yield of **1** was unchanged by increasing the Fe(TMC)(OTf)₂/Cr(OTf)₂ ratio from 1 to 10 ([Cr(OTf)₂] = 1 mM) (Fig S11), suggesting that Cr(OTf)₂ is the limiting reagent. In contrast, the yield of **1** increased to 95% when the concentration of Fe(TMC)(OTf)₂ was fixed at 1 mM and the Cr(OTf)₂ concentration was raised from 1 mM to 10 mM (Fig S12). Therefore, the % yield of **1** is dependent on the amount of Cr(OTf)₂, but not on the amount of Fe(TMC)(OTf)₂. These results can be rationalized by the O₂ activation pathway proposed in Scheme 1, in which the four electrons needed to reduce O₂ to the oxidation level of water are provided by 1 eq. Fe(TMC)(OTf)₂ and 3 eq. Cr(OTf)₂, not unlike the four redox-active centers required for O₂ activation by cytochrome oxidase.⁴ In the present case, we postulate that O₂ initially binds to the O₂-sensitive Cr(OTf)₂ to form a transient adduct (analogous to that characterized by Nam in the reaction of [Cr^{II}(TMC)Cl]⁺ with O₂²²) that is then trapped by Fe(TMC)(OTf)₂ to generate a yet unobserved Fe^{III}-O-O-Cr^{III} peroxo-bridged intermediate. This intermediate is then reduced by another 2 eq. Cr(OTf)₂ to form **1**. Thus the ca. 30% yield of **1** observed under limiting Cr conditions reflects the 1:3 stoichiometry of Fe(TMC)(OTf)₂/Cr(OTf)₂ needed to make **1**. On the other hand, under limiting Fe conditions, enough Cr–O₂ adduct is formed to react with all the available Fe(TMC)(OTf)₂ to convert the latter almost quantitatively to **1**.



Scheme 1 Proposed mechanism for formation of **1** by O₂ activation.

In conclusion, a heterobimetallic nonheme species **1** with an Fe–O–Cr core has been generated from both O₂ activation and inner-sphere electron transfer. The structure of **1** was deduced by a combination of UV-vis, resonance Raman, and X-ray absorption spectroscopic methods and ESI-MS. The O₂ activation mechanism for the formation of **1** is proposed to be analogous to that of cytochrome oxidase, where the initially formed O₂ adduct is reduced by the other three redox-active metal centers in the enzyme, demonstrating a general strategy for O₂ activation. Furthermore, **1** represents only the second example of a heterobimetallic M–O–Fe(TMC) complex, which can shed light on the effects of Lewis acidic metal centers on the redox properties of high-valent M=O species.²³ Such interactions are considered important for facilitating the oxidation of water by the CaMn₄O₅ cluster of the oxygen evolving complex in photosynthesis.^{24–26} Along these lines, Lloret-Fillol and coworkers have demonstrated the formation of a related Fe^{IV}–O–Ce^{IV} intermediate in the oxidation of water by a nonheme iron catalyst with Ce(NH₄)₃(NO₃)₆ as oxidant.²⁷

This work was supported by a grant from the US National Institutes of Health (GM-38767 to L.Q.) and a postdoctoral fellowship (GM-093479 to K.M.V.H.). XAS data were collected on Beamline X3B at the National Synchrotron Light Source, which is supported by the U.S. Department of Energy under Contract No. DE-AC02-98CH10886. Use of beamline X3B is made possible by the Center for Synchrotron Biosciences grant, P30-EB-00998, from the National Institute of Biomedical Imaging and Bioengineering. XAS data were also collected on Beamline 7-3 at the Stanford Synchrotron Radiation Lightsource, which is supported by the U.S. Department of Energy under Contract No. DE-AC02-76SF00515. Use of beamline 7-3 is supported by the DOE Office of Biological and Environmental Research, and by the National Institutes of Health, National Institute of General Medical Sciences (including P41GM103393).

References

- I. Bertini, H. Gray, E. I. Stiefel, J. S. Valentine, *Biological Inorganic Chemistry: Structure and Reactivity*, University Science Books, 2007, pp. 319–442.
- L. Que, Jr. and W. B. Tolman, *Nature*, 2008, **455**, 333–340.
- E. I. Solomon, D. E. Heppner, E. M. Johnston, J. W. Ginsbach, J. Cirera, M. Qayyum, M. T. Kieber-Emmons, C. H. Kjaergaard, R. G. Hadt and L. Tian, *Chem. Rev.*, 2014, **114**, 3659–3853.
- S. Ferguson-Miller and G. T. Babcock, *Chem. Rev.*, 1996, **96**, 2889–2908.
- T. Tsukihara, H. Aoyama, E. Yamashita, T. Tomizaki, H. Yamaguchi, K. Shinzawa-Itoh, R. Nakashima, R. Yaono and S. Yoshikawa, *Science*, 1996, **272**, 1136–1144.
- W. Jiang, D. Yun, L. Saleh, E. W. Barr, G. Xing, L. M. Hoffart, M.-A. Maslak, C. Krebs and J. M. Bollinger, *Science*, 2007, **316**, 1188–1191.
- W. Jiang, D. Yun, L. Saleh, J. M. Bollinger Jr. and C. Krebs, *Biochemistry*, 2008, **47**, 13736–13744.
- T. Chishiro, Y. Shimazaki, F. Tani, Y. Tachi, Y. Naruta, S. Karasawa, S. Hayami and Y. Maeda, *Angew. Chem. Int. Ed.*, 2003, **42**, 2788–2791.
- E. Kim, E. E. Chufán, K. Kamaraj and K. D. Karlin, *Chem. Rev.*, 2004, **104**, 1077–1134.
- E. E. Chufán, S. C. Puiu and K. D. Karlin, *Acc. Chem. Res.*, 2007, **40**, 563–572.
- R. Hotzelmann, K. Wieghardt, U. Floerke, H. J. Haupt, D. C. Weatherburn, J. Bonvoisin, G. Blondin and J. J. Girerd, *J. Am. Chem. Soc.*, 1992, **114**, 1681–1696.
- a) S. Fukuzumi, Y. Morimoto, H. Kotani, P. Naumov, Y.-M. Lee and W. Nam, *Nat. Chem.*, 2010, **2**, 756–759. b) M. Swart, *Chem. Commun.* 2013, **49**, 6650–6652. c) J. Prakash, G. T. Rohde, K. K. Meier, A. J. Jasnowski, K. M. Van Heuvelen, E. Münck and L. Que Jr., *J. Am. Chem. Soc.*, 2015, **137**, 3478–3481.
- J.-U. Rohde, J.-H. In, M. H. Lim, W. W. Brennessel, M. R. Bukowski, A. Stubna, E. Münck, W. Nam, L. Que, Jr., *Science*, 2003, **299**, 1037–1039.
- a) F. Li, Ph.D. thesis, University of Minnesota 2011. b) K. D. Koehntop, J.-U. Rohde, M. Costas and L. Que Jr., *Dalton Trans.*, 2004, 3191–3198. c) X. Shan, J.-U. Rohde, K. D. Koehntop, Y. Zhou, M. R. Bukowski, M. Costas, K. Fujisawa, L. Que, Jr., *Inorg. Chem.*, 2007, **46**, 8410–8417.
- D. M. Kurtz Jr., *Chem. Rev.*, 1990, **90**, 585–606.
- S. C. Lee and R. Holm, *J. Am. Chem. Soc.*, 1993, **115**, 11789–11798.
- J. F. Berry, E. Bill, R. García-Serres, F. Neese, T. Weyhermüller and K. Wieghardt, *Inorg. Chem.*, 2006, **45**, 2027–2037.
- D. J. Liston, B. J. Kennedy, K. S. Murray and B. O. West, *Inorg. Chem.*, 1985, **24**, 1561–1567.
- T. E. Westre, P. Kennepohl, J. G. DeWitt, B. Hedman, K. O. Hodgson and E. I. Solomon, *J. Am. Chem. Soc.*, 1997, **119**, 6297–6314.
- A. Roe, D. Schneider, R. Mayer, J. Pyrz, J. Widom and L. Que Jr., *J. Am. Chem. Soc.*, 1984, **106**, 1676–1681.
- a) J. Sanders-Loehr, W. D. Wheeler, A. K. Shiemke, B. A. Averill and T. M. Loehr, *J. Am. Chem. Soc.*, 1989, **111**, 8084–8093. b) H. Zheng, Y. Zang, Y. Dong, V. G. Young, Jr., and L. Que, Jr., *J. Am. Chem. Soc.* 1999, **121**, 2226–2235
- J. Cho, J. Woo and W. Nam, *J. Am. Chem. Soc.*, 2010, **132**, 5958–5959.
- a) S. Fukuzumi, *Coord. Chem. Rev.*, 2013, **257**, 1564–1575. b) W. Nam, Y.-M. Lee, S. Fukuzumi, *Acc. Chem. Res.* 2014, **47**, 1146–1154.
- J. Yano, V. Yachandra, *Chem. Rev.* 2014, **114**, 4175–4205.
- P. E. Siegbahn, *Acc. Chem. Res.*, 2009, **42**, 1871–1880
- E. Y. Tsui, J. S. Kanady and T. Agapie, *Inorg. Chem.*, 2013, **52**, 13833–13848
- Z. Codolà, L. Gómez, S. T. Kleespies, L. Que Jr., M. Costas and J. Lloret-Fillol, *Nat. Commun.*, 2015, **6**, 5865 10.1038/comms6865.

TOC graphic

